

NbS₂: A Promising *p*-Type Ohmic Contact for Two-Dimensional Materials

Xiang Ding,¹ Sa Zhang,¹ Mei Zhao,¹ Yang Xiang,¹ Kelvin H.L. Zhang,² Xiaotao Zu,^{1,*}
Sean Li,³ and Liang Qiao^{1,3,†}

¹School of Physics, University of Electronic Science and Technology of China, Chengdu 610054, China

²State Key Laboratory of Physical Chemistry of Solid Surfaces, College of Chemistry and Chemical Engineering, Xiamen University, Xiamen 361005, China

³School of Materials, University of New South Wales, Sydney, 2052 NSW, Australia

(Received 18 July 2019; revised manuscript received 24 October 2019; published 30 December 2019)

Achieving Ohmic contact for two-dimensional- (2D) based electronics is important yet challenging. Here through first-principles calculations, we predict that a NbS₂ monolayer is an excellent electrode for *p*-type Ohmic contacts for 2D materials. Dipole analysis indicates van der Waals interfacial interaction and high electrode work function are critical for asymmetric dipole compensation to maintain the Ohmic contact for NbS₂/BP and NbS₂/WSe₂. *p*-type Ohmic contacts for both heterostructures are independent of gating up to very large electric field (7 V/nm) suggesting good stability for device applications. Our work provides a practical strategy to realize stable *p*-type Ohmic contacts for future 2D nanoelectronics.

DOI: 10.1103/PhysRevApplied.12.064061

I. INTRODUCTION

Ohmic contact is essential for electronic devices. Yet, due to intrinsic and extrinsic limitations, such as mismatch of work functions, surface defects, interfacial states etc., achieving good Ohmic contact in electrode-semiconductor interfaces represents a challenging task [1,2]. For traditional Si-based FETs, it has been well established that tunneling through degenerate doping or formation of metallic metal silicide are critical to realize Ohmic metal-Si contact, which also ensures a small contact resistance that is independent of gate voltage [3,4]. Unfortunately, the interfaces between metal and two-dimensional semiconductors (2DSs) are mostly Schottky in nature due to intrinsic smaller electron affinity and larger ionization potential of 2DSs than that of three-dimensional (3D) channel materials [5]. This is further exacerbated by the lack of controllable and sustainable doping strategies in 2DSs, thus making Ohmic contact in metal-2DS systems extremely difficult [6].

Currently, achieving quasi-Ohmic contact in metal-2DS systems relies on a large global gate voltage to eliminate the Schottky barrier height (SBH) [2,7]. However, for the most widely used back-gate (and even some top-gate) FET setups, gating essentially plays a “dual” role [2,4]. On one hand, it electrically injects or depletes channel carriers to perform an on/off switch. On the other hand, since back-gate covers entire channel area including

regions below source and drain electrodes, thus during on and off switch, gating also inevitably affects SBH for both source-channel and drain-channel interfaces (side effects). Unlike Si-based FETs with little dependence of SBH on gating, 2DS-based FETs are more sensitive to gating [4]. It has been recently demonstrated that this “dual” function of gating often occurs simultaneously, without proper and careful data extraction, it can result in misleading interpretation of device performance [8,9]. Furthermore, large gating voltage can even lead to Ohmic- to Schottky-type conversion in metal-2DS systems [10,11]. Therefore, from a device-functioning perspective, in analogy to Si-based FETs, it is necessary to develop 2DS-based FETs that are naturally Ohmic with less dependence on gating.

Meanwhile, alternative strategies have also been developed to reduce SBH in metal-2DS systems, i.e., choosing metals with a suitable work function [12], surface chemical doping [13], inserting a 2D buffer layer [14,15], and introducing metallic 2D materials [16]. Recently, van der Waals (vdW) metal-semiconductor junctions have been demonstrated to significantly reduce the Fermi-level pinning and approach the Schottky-Mott limit for MoS₂ [17,18], yet these 2D contacts are not strictly Ohmic, small SBHs (20–67 meV) still exist due to the mismatch of the metal’s work function. Therefore, to date, only very limited examples of Ohmic metal-2DS contacts have been experimentally realized, such as Au/Pd/MoS₂ [19], permalloy/MoS₂ [20], *h*-BN encapsulated Pd/WSe₂ [21] (Table SI in Supplemental Material [15,17–20,22–34]). Moreover, current 2DS FETs are mostly *n* type, identifying stable *p*-type metal-2DS systems is necessary for

*zuxt@uestc.edu.cn

†liang.qiao@uestc.edu.cn

constructing all 2DS-based complementary logic circuit inverters for device application.

In this work, through density-functional-theory (DFT) calculation we demonstrate monolayer NbS₂ to be a promising 2D electrode for 2DSs to achieve intrinsic and stable Ohmic contacts with *p*-type nature. Band-structure investigation indicates that an ultra-high work function of NbS₂ results in the Fermi level crossing the valence bands of adjacent 2DSs (BP and WSe₂), thus stabilizing a robust *p*-type and Ohmic contact for NbS₂/BP and NbS₂/WSe₂ heterostructures. Comparative dipole analysis indicates sufficiently large work function is critical for the compensation of asymmetric interfacial dipole-induced work-function reduction to thus maintain the Ohmic contact. More importantly, the *p*-type Ohmic contacts in both metal-2DS junctions are independent of gating up to very large electric field (7 V/nm), suggesting good electric stability for device applications. Our results provide illuminative insight to identify effective strategy to achieve intrinsic and electrical stable *p*-type Ohmic contact for all 2DS-based nanoelectronics.

II. COMPUTATIONAL METHOD

The present calculations are based on DFT as implemented in the Vienna *ab initio* simulation package (VASP) [35], using the projector augmented-wave (PAW) method [36]. Both the Perdew-Burke-Ernzerhof (PBE) version of the generalized gradient approximation (GGA) [37–39] and hybrid exchange-correlation functional (HSE06) [40–42] are used for exchange correlation. VdW interactions are taken into account through the optB86b-vdW functional to minimize errors when calculating structural parameters and binding energies [43]. The combination of PBE and optB86b-vdW functional is shown to reproduce the experimental geometries well and the theoretical equilibrium volumes of the studied bulk materials are no more than 1.5% larger than the experiment, as listed in Table I. A vacuum space larger than 20 Å is introduced to 2D slab models to ensure decoupling between periodically repeated systems. The energy cutoff is set to 500 eV for the plane-wave expansion of the projector-augmented waves in the self-consistent calculations. Each system is fully relaxed with residual forces smaller than 0.01 eV/Å and the total-energy change is less than 10⁻⁵ eV during

the structural optimization. A dipole correction is applied to avoid spurious interactions between periodic images of the slab [46].

III. RESULTS AND DISCUSSION

NbS₂ shows the highest intrinsic work function (approximately 6.2 eV) among the available metallic 2D materials and 3D metals (Table SII in Supplemental Material [22, 47–57]). It is also much higher than the value for common electrode graphene (4.6 eV) [58]. The large work function of H-NbS₂ is determined by crystal symmetry and orbital filling. Generally, the electronic structures of transition metal dichalcogenides (TMDs) are under the combined influence of crystal structures and the filling of *d* shells. The typical “H” and “T” phases corresponds to the trigonal prismatic and octahedral coordination. Such different crystal fields result in different splitting of metal *d* levels. For H phase, *d*-electron levels split into a low-energy singlet *a*₁, a medium-energy doublet *e*, and a high-energy doublet *e'*. While for T phase, the *d* orbitals split into a triplet *t*_{2g}, and a doublet *e*_g [59], as shown in Fig. 1. Then, *d*-shell filling determines the electronic properties and work functions of TMDs. For example, a Nb atom has one extra electron when forming NbS₂ with S atoms, this electron fills the lowest *d* subband in both the H and T phases, which leads to an incomplete filling. Therefore, both H- and T-NbS₂ exhibit metallic behavior. As for MoS₂ and WSe₂, in which the transition metal atom has two extra electrons, the fully filled *a*₁ subband in the H phase makes it semiconducting, while the incomplete filling of *t*_{2g} in the T phase makes it metallic (see Fig. S1 in Supplemental Material [22]). The rule can be extended to other TMDs with a different valence electron in those two phases. The main reason why H-phase NbS₂ has a large work function is that it possesses trigonal prismatic symmetry. Since the first two subbands (*a*₁ and *e*) in the H phase have a sizable energy gap up to approximately 1 eV) [60], the metallic TMDs with H phase tend to possess much larger work function than T phase, such tendency is well presented in Liu’s work [58]. In the following discussion, we use H-NbS₂ for heterostructure calculation and take NbS₂ to denote H-NbS₂, since experimentally synthesis of T-phase NbS₂ is quite rare [61].

TABLE I. Experimental [44,45] and calculated lattice parameters, work functions (WF) of NbS₂, and valence-band maximum (VBM) and conduction-band minimum (CBM) of WSe₂ and BP.

	Expt. bulk (Å)		Calc bulk (Å)		WF (eV)	VBM (eV)	CBM (eV)
	<i>a</i> (<i>b</i>)	<i>c</i>	<i>a</i> (<i>b</i>)	<i>c</i>			
NbS ₂	3.33	17.90	3.32	18.15	6.20
WSe ₂	3.29	12.99	3.30	13.10	...	5.18	3.55
BP	3.31 (4.38)	10.50	3.33 (4.35)	10.52	...	4.95	4.42

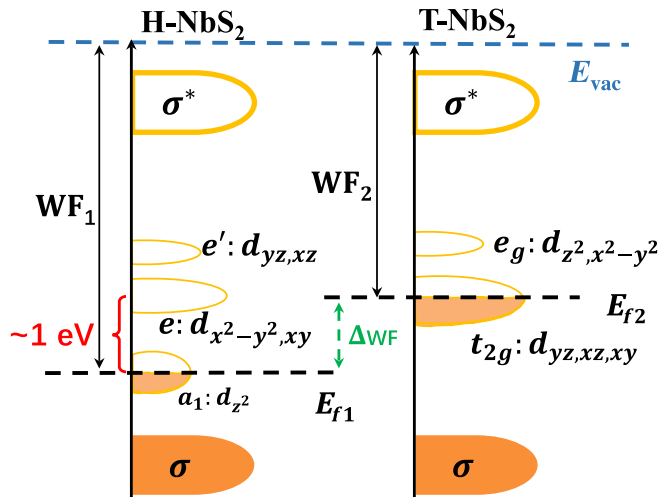


FIG. 1. Electronic properties and work-function comparison between two typical metallic TMDs H-NbS₂ (left) and T-NbS₂ (right) with transition metal *d* orbitals splitting in the trigonal prismatic structure and the octahedral structure between bonding (σ) and antibonding (σ^*) states. Vacuum level is indicated by dashed blue line.

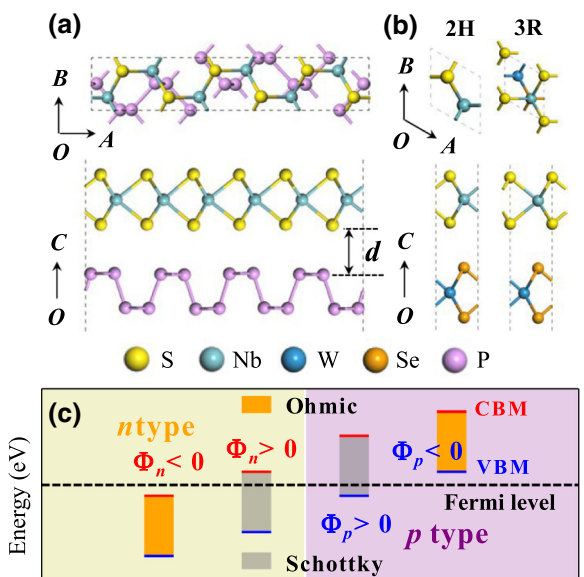
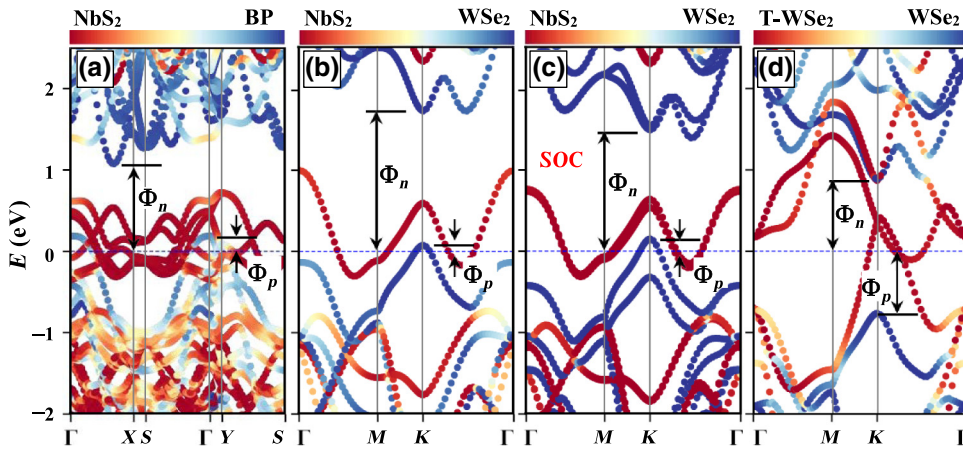


FIG. 2. Top (upper panel) and side (lower panel) views of (a) NbS₂/BP and (b) NbS₂/WSe₂ interface systems. For (b), the left panel is 2H stacking and the right panel is 3R stacking. The interlayer distance is indicated by d . (c) Illustration of contact type and favorable carrier type.

We then consider ideal 2D metal-semiconductor interfaces taking the NbS₂ monolayer as a metallic electrode and the BP or WSe₂ monolayer as the channel material [Figs. 2(a) and 2(b)]. To deal with lattice mismatch, a widely used strategy of accommodating the lattice of metallic layers to match the lattice parameters of semiconducting layers is adopted [62]. For NbS₂/WSe₂ interfaces, the lattice mismatch can be controlled below 1% in their 1×1 primitive cells due to their close lattice constants. For the NbS₂/BP system, a supercell model (1×4 supercell of BP monolayer and $1 \times 3\sqrt{3}$ supercell of NbS₂ monolayer) is used, as shown in Fig. 2(a). Both 2H and 3R stacking orders are considered for NbS₂/WSe₂ interfaces according to their bulk counterparts, while in the discussion we mainly focus on the 3R geometry (results of 2H stacking can be found in Supplemental Material [22]). The equilibrium interface distance d is defined as the average out-of-plane distance between the S atoms at the bottom of NbS₂ and atoms at the top of WSe₂ and BP. SBH is defined by the energy difference between the Fermi level of the composite system and conduction-band minimum (CBM) or valence-band maximum (VBM) of the respective semiconductor [63], and can be extracted from band alignments, as illustrated in Fig. 2(c). If the Fermi level within the bandgap is closer to the CBM, an *n*-type Schottky barrier (electron barrier, Φ_n) is formed. Otherwise, a *p*-type Schottky barrier (hole barrier, Φ_p) is formed. Furthermore, if the Fermi level falls into conduction band ($\Phi_n < 0$) or valence band ($\Phi_p < 0$), an Ohmic contact is formed [7].

To study the electronic structure of those interfaces, we calculate their projected band structures. As shown in Fig. 3(a), NbS₂/BP heterostructure exhibits $\Phi_p \sim -0.19$ eV, indicating an Ohmic contact. In addition, compared with isolated BP monolayer [Fig. S2(a), Supplemental Material [22]], we find only the bottom part of the conduction band of BP in the NbS₂/BP heterostructure shows modification when coupled with 2D electrode NbS₂, and the rest of the band structure remains unchanged. This is quite different from previously studied 3D metal-BP systems in which BP are strongly hybridized with metals, indicating the formation of covalent bonds [64]. vdW interaction in here plays an important role in reducing the interface states formed at metal-2DS junction.

Similar to the NbS₂/BP interface, the electronic structure of NbS₂/WSe₂ is mostly preserved upon the interface formation. From the projected band structure, we obtain a Φ_p of -0.11 eV and a Φ_n of 1.73 eV for NbS₂/WSe₂ system, also suggesting a *p*-type Ohmic contact formation, consistent with previous work [58]. From carrier-injection point of view, this large SBH difference between *n*-type and *p*-type carriers in the NbS₂/WSe₂ interface is expected to suppress the ambipolar behavior in WSe₂-based FETs, which is a prerequisite for complementary logic devices. In addition, we also consider the spin-orbit coupling (SOC) and its impact on the SBH of NbS₂/WSe₂ since the monolayer of WSe₂ is shown to exhibit strong SOC due to its heavier element and quantum-confinement-induced inversion symmetry being broken. The calculated SOC corrected band structure in Fig. 3(c) indicates Φ_p becomes



more negative and still preserves the *p*-type Ohmic contact. In addition, 2H-stacked NbS₂/WSe₂ exhibits similar *p*-type Ohmic contact, as shown in Fig. S3(a) (Supplemental Material [22]).

To highlight the critical role of metal work function, here we select another metallic 2D electrode with smaller work-function values, i.e., T-phase WSe₂ (4.5 eV). Figure 3(d) shows the T-WSe₂/WSe₂ interface leads to the Fermi level being well above the VBM of WSe₂ due to smaller work function of T-WSe₂. This is in contrast to the NbS₂/WSe₂ interface whose Fermi level is pinned well below the VBM of the WSe₂ [Fig. 3(b)].

For Schottky barrier prediction, aligning the band edges of the metal and the semiconductor according to vacuum levels has been widely accepted as the Schottky-Mott rule. Over the last decades, however, many experimental studies have demonstrated the general deviation of the ideal vacuum alignment rule and have revealed that significant interface dipoles are formed at metal-semiconductor interfaces [14,65]. The interface dipole is related to the charge transfer at the interface, which can be directly visualized by calculating the plane-averaged electron density difference $\Delta\rho$, which is defined as

$$\Delta\rho = \rho_{\text{bilyaer}} - \rho_{\text{layer1}} - \rho_{\text{layer2}},$$

FIG. 3. Projected band structures of NbS₂ stacks with (a) BP and WSe₂ without (b), and (c) with consideration of SOC. (d) Projected band structures of T-WSe₂ stacks with WSe₂. The color map at the top indicates the magnitude of the projection.

where ρ_{bilyaer} and $\rho_{\text{layer1(2)}}$ correspond to the charge density of the heterostructure and the isolated semiconducting (metallic) monolayer. The $\Delta\rho$ distribution of NbS₂/WSe₂, T-WSe₂/WSe₂ and NbS₂/BP, are shown in Figs. 4(a) and 4(b) and Fig. S4 (Supplemental Material [22]), respectively, from which electron transfer at the metal-semiconductor interfaces is clearly demonstrated. Such a charge transfer is a pure electronic effect from the charge redistribution in the interface, known as a pillow effect [62]. Pauli exchange in here plays an important role in pushing electrons back into the metal sides, and thus yields an interface dipole that decreases the surface work function [66]. For NbS₂/BP or NbS₂/WSe₂, an asymmetric $\Delta\rho$ pattern in the interface zone indicates a net significant interface dipole formation, as indicated by green arrows. The observed electron accumulation (in NbS₂ side) and depletion (in BP or WSe₂ side) suggest electrons are transferred from WSe₂ (BP) to NbS₂. In contrast, Fig. 4(b) shows a more complex but relatively symmetric $\Delta\rho$ pattern in the T-WSe₂/WSe₂ interface zone. The complexity pattern indicates the formation of more local dipoles and the mirror symmetry suggests those local dipoles are in antiparallel alignments [green arrows in Fig. 4(b)]. As a result, the total net dipole in such a pattern is negligible.

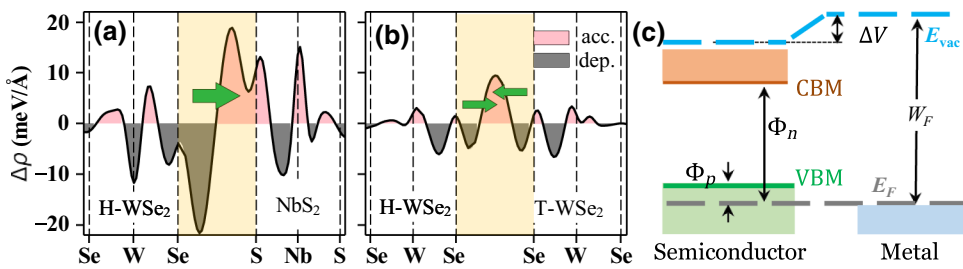


FIG. 4. (a),(b) are plane-averaged electron density difference ($\Delta\rho = \rho_{\text{bilyaer}} - \rho_{\text{layer1}} - \rho_{\text{layer2}}$) corresponding to NbS₂/WSe₂ and T-WSe₂/WSe₂ interfaces. Red and gray color filled areas represent charge accumulation (acc.) and depletion (dep.) zones, respectively. Dotted lines indicate average *z* positions of atomic planes and the interface zones are highlighted in yellow. Local dipoles are indicated by green arrows. (c) Illustration of metal-semiconductor interface band alignment of NbS₂/WSe₂.

Net interface dipole can induce an interface potential step ΔV via Helmholtz relation [65], resulting in deviation from the ideal Schottky-Mott rule at the vdW interacted metal-semiconductor interface. When taking the interface dipole into account, for the NbS₂/WSe₂ interface, as depicted in Fig. 4(c), the SBH for holes can be modified as $\Phi_p = E_v - W_M + \Delta V$, where E_v is the VBM of the semiconductor with respect to the vacuum energy, W_M is the work function of the metal, and ΔV is the potential step formed at the metal-semiconductor interfaces [14]. Generally, the potential step ΔV can be calculated by solving the Poisson equation with $\Delta\rho(r)$ as the source, however, the accuracy of this method depends strongly on boundary conditions [65]. Alternatively, ΔV can also be obtained without solving the Poisson equation by using $\Delta V = W_M - W_{ads/M}$, where $W_{ads/M}$ is the work function of the metal surface covered with semiconductors (Fig. S5 in Supplemental Material [22]) [14]. Thus a positive ΔV can result in a reduction of the effective work function. Considering a bandgap (E_g) of the semiconductor, then SBH for electrons is given by $\Phi_n = E_g - \Phi_p$. Table II gives the interface potential steps of studied contact systems using this method. It is seen that the $\Phi_p(\Phi_n)$ extracted from this charge-transfer analysis are in good agreement with band-structure calculations.

From above discussion we show that vdW contact in metal-2DS junctions leads to weak interfacial interaction, which is expected to suppress the metal-induced gap states in metal-2DS junctions and helpful for achieving Ohmic contact [58]. On the other hand, the Pauli exchange interaction in vdW contacted metal-2DSs tends to modify $\Delta\rho$ and results in a net dipole, thus leading to unintentional modification of metal work function (reduction in this case), which may hinder the formation of Ohmic contact. These competing effects strongly influence the SBH of metal-semiconductor contacts, and plays an important role in the physics of 2D-semiconductor devices. In our case, we find NbS₂/BP and NbS₂/WSe₂ interfaces have a stronger net interface dipole, which is expected to induce work-function reduction to NbS₂. Even though the intrinsically large work-function value of NbS₂ provides adequate room for the compensation of interface dipole-induced work-function reduction, thus maintaining an Ohmic nature for the contact. In addition, for the T-WSe₂/WSe₂ interface, the observed much more

symmetric $\Delta\rho$ pattern and negligible net dipole account for the very small changes of work function for metallic T-WSe₂ in the T-WSe₂/WSe₂ interface (Table II). Farmanbar *et al.* also report a symmetric $\Delta\rho$ pattern in the metal-semiconductor interface gives a smaller work-function reduction [62].

In order to evaluate the stability of the SBH of metal-2DS contacts under external electric voltage for potential complementary logic circuit applications, we study the dependence of the Φ_n and Φ_p for three typical systems as functions of gate voltage, e.g., NbS₂/WSe₂ and T-WSe₂/WSe₂ [Figs. 5(a) and 5(b)] as well as NbS₂/BP [Fig. S4(b) in Supplemental Material [22]], respectively.

It is clearly seen that both NbS₂/BP and NbS₂/WSe₂ show similar weak electric field dependence of SBH (Φ_n and Φ_p) and the *p*-type Ohmic character is quite stable ($|\Phi_p|$ always smaller than $|\Phi_n|$) throughout the entire operation electric field (-7 to 7 V/nm). Generally, it is reported that large gate voltage can lead to Ohmic- to Schottky-type conversion in metal-2DS systems [10,11]. Therefore, maintaining a robust Ohmic contact even under strong field is very important for practical device applications. In contrast, the large variation of SBH values for T-WSe₂/WSe₂ suggests a much stronger external electric field dependency than NbS₂-based contacts. This strong SBH-external electric field correlation can even drastically alter the nature of the metal-semiconductor contacts, for example, as the applied voltage value becomes negative, a *p*- to *n*-type conversion occurs at -3 V/nm for T-WSe₂/WSe₂. Similar types of conversion phenomena have also been reported in graphene/BP and T-MoS₂/MoS₂ systems where *p*- to *n*-type conversion occurs at 1.5 and -4 V/nm, respectively [7,57]. Thus, these results demonstrate that the metallic monolayer NbS₂ is more effective than other conventional 2D electrodes to realize a more stable Ohmic contact that is almost independent of external voltage up to very large values for device applications.

To more deeply understand the influence of external field on interface charge transfer, we further calculate the electric-field-dependent dipole redistribution, as shown in Figs. 5(c) and 5(d). For the NbS₂/WSe₂ interface, without electric field, the electron-density difference curve ($\Delta\rho$) for the interface zone (yellow highlight) is highly asymmetric along the vdW gap with a large dipole moment. This static charge distribution shows further slight “up

TABLE II. Calculated equilibrium interfacial distances (d), binding energies (E_b) of studied interfaces, electrostatic potential step (ΔV), *p*- (*n*-) type Schottky barrier height $\Phi_{p(n)B}$ extract from band diagrams, and *p*- (*n*-) type Schottky barrier height $\Phi_{p(n)M}$ extract from dipole-modified the Schottky-Mott model.

Stacking configurations	$d(\text{\AA})$	$E_b(\text{meV}/\text{\AA}^2)$	$\Delta V(\text{eV})$	$\Phi_{pB}(\text{eV})$	$\Phi_{nB}(\text{eV})$	$\Phi_{pM}(\text{eV})$	$\Phi_{nM}(\text{eV})$
NbS ₂ /WSe ₂ (3R)	3.02	-28.7	0.91	-0.11	1.73	-0.11	1.74
NbS ₂ /WSe ₂ (2H)	3.05	-28.7	0.87	-0.10	1.75	-0.15	1.78
T-WSe ₂ /WSe ₂	3.14	-26.6	-0.02	0.76	0.89	0.67	0.96

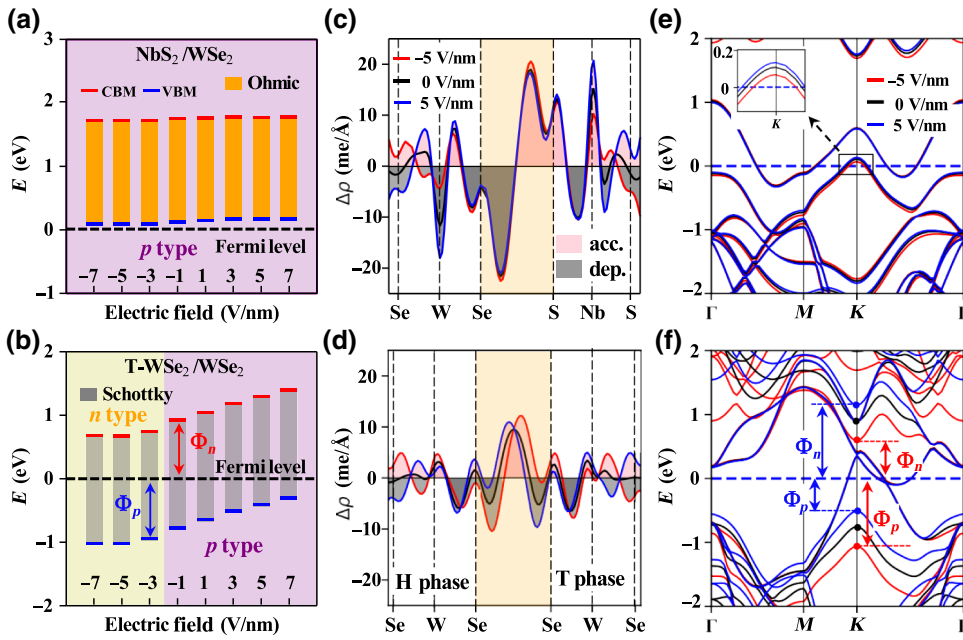


FIG. 5. Evolution of the SBH as a function of the external field for (a) NbS₂/WSe₂ and (b) T-WSe₂/WSe₂ contact. Evolution of $\Delta\rho$ under different applied field for (c) NbS₂/WSe₂ and (d) T-WSe₂/WSe₂, where applied electrostatic fields -5, 0, and 5 V/nm are indicated by red, black, and blue solid lines. Influence of an external electric filed on $\Delta\rho$ corresponding to (e) NbS₂/WSe₂ and (f) T-WSe₂/WSe₂ interfaces. Dotted lines indicate average z positions of atomic planes and the interface zones are highlighted in yellow. Red and gray color filled areas represent charge accumulation and depletion zones, respectively.

(down) shift” for the peak portion and “down (up) shift” for the valley portion under negative (positive) field. This vertical response of $\Delta\rho$ to external field is generally trivial, indicating relatively weak electric-field-induced dipole redistribution at the NbS₂/WSe₂ interface. As a result, the shape of $\Delta\rho$ in the interface zone remains unchanged, leading to negligible change for the net interface dipole magnitude driven by applied field. In contrast, the $\Delta\rho$ of T-WSe₂/WSe₂ shows a more symmetric pattern leading to an overall smaller static net dipole moment. This symmetric dipole, however, shows significant “right (left) shift” under a negative (positive) field. This horizontal response of $\Delta\rho$ to external field is stronger, leading to a stronger dipole redistribution at this interface.

The weak (strong) electric-field-induced dipole redistribution for the NbS₂/WSe₂ (T-WSe₂/WSe₂) interface can be interoperated from a band-structure point of view. As shown in Figs. 5(e) and 5(f), the Fermi level of metallic NbS₂ and T-WSe₂ are unaffected by electric field. However, the band-edge positions for semiconductor WSe₂ show different electric field response when contacting these two types of electrodes. For the NbS₂/WSe₂ interface, both VBM and CBM of WSe₂ are less dependent on field, while for the case of T-WSe₂/WSe₂, both VBM and CBM show significantly change, especially along high-symmetry K point. The change of band alignment is expected to result in the observed electric-field-induced dipole redistribution. This also accounts for the observed independence of SBH on external field for NbS₂-based metal-2DS contacts in Figs. 5(a) and 5(c).

Calculation based on the HSE06 functional show similar results, as shown in Fig. S6 (Supplemental Material [22]).

Both GGA and HSE give Ohmic contact for NbS₂/WSe₂ and Schottky contact for T-WSe₂/WSe₂. Although there are differences in the absolute value of $\Delta\rho$ [Figs. S6(b) and S6(e) in Supplemental Material [22]], calculation based on the HSE functional gives a similar asymmetric (symmetric) $\Delta\rho$ pattern and interface dipole for NbS₂/WSe₂ (T-WSe₂/WSe₂) systems. Both methods give generally the same trend when imposing an external electric field. Other discrepancies between these two methods, such as specific SBH values (Φ_n and Φ_p), is due to the corrected larger bandgap values in the HSE frame.

Generally, the strategy of applied external field (gating) is often used to either tune carrier concentration or tune SBH. However, for low-dimensional materials, particularly for back-gated FETs with gating cover all areas of source, drain, and channel [8], the “dual” function of gating tends to occur simultaneously. It is expected that the simultaneous modification of SBH and carrier concentration may lead to data interpretation for FETs being more complicated. Yet, due to a lack of appropriate data-processing approaches, the “dual” function of gating in back-gated FETs is often ignored. Recently, Joseph *et al.* point out that ignorance of this fact can lead to incorrect data extraction, and thus wrong interpretation of the device’s electrical behavior [4]. Ashish *et al.* also developed a model based on Landauer’s formalism to analyze BP-based transistors. Yet the universality of such a model need to be improved to extend to other material systems [9]. Therefore, it will be more meaningful if this “dual” function can be separated and independently controlled. In this work, large work-function-induced weak electric field dependence of SBH for NbS₂-based metal-2DS systems

allows straightforward control of the intrinsic electronic properties (such as carrier concentration, mobility, device efficiency, etc.) for electric gating study of these emerging 2D materials.

Even though, we have to point out that NbS₂ cannot guarantee Ohmic contacts to all of those 2D materials, especially for those 2D materials with large bandgap. It is obvious in Vinod's recent review work [5], materials with large bandgap tend to have large ionic potential, i.e., large VBM. From this point of view, although NbS₂ has the largest work function, it cannot satisfy the Ohmic contact condition with all 2D materials. To conform this, we also calculate the electronic properties of NbS₂/*h*-BN heterostructure, and find the contact between NbS₂ and large-gaped *h*-BN to be Schottky type, as shown in Fig. S7 (Supplemental Material [22]). However, *h*-BN is a widely used encapsulation layer to protect channel materials from degradation in air [67]. From this perspective, the absence of Ohmic contact between the electrode and *h*-BN is in fact a good property for 2D devices, which means the encapsulation layer cannot be a conduction channel for them.

IV. CONCLUSION

In summary, we discuss the origin of the large work function of NbS₂ in the frame of crystal field, and demonstrate through first-principles calculations that trigonal prismatic coordinated NbS₂ is a promising 2D electrode to achieve Ohmic contacts for WSe₂ and BP-based FETs. Ultra-large work function of NbS₂ provides adequate room to compensate asymmetric interface dipole-induced work-function reduction, thus pinning the VBM of the 2D semiconductor above its Fermi level to maintain a robust Ohmic nature for this *p*-type contact. We further show the obtained *p*-type Ohmic contact is extremely stable up to even very large electric field, which enables the common "dual function" of gating in back-gated devices to achieve more straightforward control of the intrinsic electronic properties to be avoided. Our work demonstrates by choosing an appropriate electrode, the common problem of Ohmic to Schottky contact conversion and common "dual function" of gating can be avoided, thus paving the way for future 2D nanoelectronics.

ACKNOWLEDGMENTS

L. Qiao is supported by National Natural Science Foundation of China (Grant No. 11774044). This work is supported by the NSAF Joint Foundation of China (Grant No. U1630126). Theoretical calculations are performed using the supercomputer resources at TianHe-1 located at National Supercomputer Center in Tianjin.

- [1] Y. Liu, Y. Huang, and X. Duan, Van der Waals integration before and beyond two-dimensional materials, *Nature* **567**, 323 (2019).
- [2] D. S. Schulman, A. J. Arnold, and S. Das, Contact engineering for 2D materials and devices, *Chem. Soc. Rev.* **47**, 3037 (2018).
- [3] C. H. Ahn, A. Bhattacharya, M. Di Ventra, J. N. Eckstein, C. D. Frisbie, M. E. Gershenson, A. M. Goldman, I. H. Inoue, J. Mannhart, A. J. Millis, A. F. Morpurgo, D. Natelson, and J.-M. Triscone, Electrostatic modification of novel materials, *Rev. Mod. Phys.* **78**, 1185 (2006).
- [4] J. R. Nasr, D. S. Schulman, A. Sebastian, M. W. Horn, and S. Das, Mobility deception in nanoscale transistors: An untold contact story, *Adv. Mater.* **31**, 1806020 (2019).
- [5] V. K. Sangwan and M. C. Hersam, Electronic transport in two-dimensional materials, *Annu. Rev. Phys. Chem.* **69**, 299 (2018).
- [6] R. Kappera, D. Voiry, S. E. Yalcin, B. Branch, G. Gupta, A. D. Mohite, and M. Chhowalla, Phase-engineered low-resistance contacts for ultrathin MoS₂ transistors, *Nat. Mater.* **13**, 1128 (2014).
- [7] J. E. Padilha, A. Fazzio, and A. J. R. da Silva, Van der Waals Heterostructure of Phosphorene and Graphene: Tuning the Schottky Barrier and Doping by Electrostatic Gating, *Phys. Rev. Lett.* **114**, 066803 (2015).
- [8] A. Prakash, H. Ilatikhameneh, P. Wu, and J. Appenzeller, Understanding contact gating in Schottky barrier transistors from 2D channels, *Sci. Rep.* **7**, 12596 (2017).
- [9] A. V. Penumatcha, R. B. Salazar, and J. Appenzeller, Analysing black phosphorus transistors using an analytic Schottky barrier MOSFET model, *Nat. Commun.* **6**, 8948 (2015).
- [10] F. Zhang, W. Li, Y. Ma, Y. Tang, and X. Dai, Tuning the Schottky contacts at the graphene/WS₂ interface by electric field, *RSC Adv.* **7**, 29350 (2017).
- [11] J. Wu, H. Yuan, M. Meng, C. Chen, Y. Sun, Z. Chen, W. Dang, C. Tan, Y. Liu, J. Yin, Y. Zhou, S. Huang, H. Q. Xu, Y. Cui, H. Y. Hwang, Z. Liu, Y. Chen, B. Yan, and H. Peng, High electron mobility and quantum oscillations in non-encapsulated ultrathin semiconducting Bi₂O₂Se, *Nat. Nanotechnol.* **12**, 530 (2017).
- [12] C. Gong, L. Colombo, R. M. Wallace, and K. Cho, The unusual mechanism of partial Fermi level pinning at metal–MoS₂ interfaces, *Nano Lett.* **14**, 1714 (2014).
- [13] H. Fang, S. Chuang, T. C. Chang, K. Takei, T. Takahashi, and A. Javey, High-performance single layered WSe₂ *p*-FETs with chemically doped contacts, *Nano Lett.* **12**, 3788 (2012).
- [14] M. Farmanbar and G. Brocks, Controlling the Schottky barrier at MoS₂/metal contacts by inserting a BN monolayer, *Phys. Rev. B* **91**, 161304 (2015).
- [15] X. Cui, E. M. Shih, L. A. Jauregui, S. H. Chae, Y. D. Kim, B. C. Li, D. Seo, K. Pistunova, J. Yin, J. H. Park, H. J. Choi, Y. H. Lee, K. Watanabe, T. Taniguchi, P. Kim, C. R. Dean, and J. C. Hone, Low-temperature ohmic contact to monolayer MoS₂ by van der Waals bonded Co/*h*-BN electrodes, *Nano Lett.* **17**, 4781 (2017).

- [16] R. Wu, Q. Tao, W. Dang, Y. Liu, B. Li, J. Li, B. Zhao, Z. Zhang, H. Ma, G. Sun, X. Duan, and X. Duan, Van der Waals epitaxial growth of atomically thin 2D metals on dangling-bond-free WSe₂ and WS₂, *Adv. Funct. Mater.* **29**, 1806611 (2019).
- [17] Y. Liu, J. Guo, E. Zhu, L. Liao, S.-J. Lee, M. Ding, I. Shakir, V. Gambin, Y. Huang, and X. Duan, Approaching the Schottky–Mott limit in van der Waals metal–semiconductor junctions, *Nature* **557**, 696 (2018).
- [18] Y. Wang, J. C. Kim, R. J. Wu, J. Martinez, X. Song, J. Yang, F. Zhao, A. Mkhoyan, H. Y. Jeong, and M. Chhowalla, Van der Waals contacts between three-dimensional metals and two-dimensional semiconductors, *Nature* **568**, 70 (2019).
- [19] X. Zheng, A. Calò, E. Albisetti, X. Liu, A. S. M. Alharbi, G. Arefe, X. Liu, M. Spieser, W. J. Yoo, T. Taniguchi, K. Watanabe, C. Aruta, A. Ciarrocchi, A. Kis, B. S. Lee, M. Lipson, J. Hone, D. Shahrjerdi, and E. Riedo, Patterning metal contacts on monolayer MoS₂ with vanishing Schottky barriers using thermal nanolithography, *Nat. Electron.* **2**, 17 (2019).
- [20] W. Wang, Y. Liu, L. Tang, Y. Jin, T. Zhao, and F. Xiu, Controllable Schottky barriers between MoS₂ and permalloy, *Sci. Rep.* **4**, 6928 (2014).
- [21] S. Xu, Z. Wu, H. Lu, Y. Han, G. Long, X. Chen, T. Han, W. Ye, Y. Wu, J. Lin, J. Shen, Y. Cai, Y. He, F. Zhang, R. Lortz, C. Cheng, and N. Wang, Universal low-temperature Ohmic contacts for quantum transport in transition metal dichalcogenides, *2D Mater.* **3**, 021007 (2016).
- [22] See Supplemental Material at <http://link.aps.org/supplemental/10.1103/PhysRevApplied.12.064061> for original band structures of monolayers, results of 2H-stacked heterostructure, as well as the results based on the HSE06 functional.
- [23] S. Das and J. Appenzeller, WSe₂ field effect transistors with enhanced ambipolar characteristics, *Appl. Phys. Lett.* **103**, 103501 (2013).
- [24] F. Ali, F. Ahmed, Z. Yang, I. Moon, M. Lee, Y. Hassan, C. Lee, and W. J. Yoo, Energy dissipation in black phosphorus heterostructured devices, *Adv. Mater. Interfaces* **6**, 1801528 (2019).
- [25] C.-H. Wang, J. A. C. Incorvia, C. J. McClellan, A. C. Yu, M. J. Mleczko, E. Pop, and H. S. P. Wong, Unipolar *n*-type black phosphorus transistors with low work function contacts, *Nano Lett.* **18**, 2822 (2018).
- [26] S. Das, H.-Y. Chen, A. V. Penumatcha, and J. Appenzeller, High performance multilayer MoS₂ transistors with scandium contacts, *Nano Lett.* **13**, 100 (2013).
- [27] M. V. Kamalakar, B. N. Madhushankar, A. Dankert, and S. P. Dash, Low Schottky barrier black phosphorus field-effect devices with ferromagnetic tunnel contacts, *Small* **11**, 2209 (2015).
- [28] I. Liao, D. Barroso, A. E. Nguyen, N. Duong, Q. B. Yurek, C. S. Merida, P. Peña, I. H. Lu, M. D. Valentin, G. Stecklein, and L. Bartels, Hybrid single-layer/bulk tungsten diselenide transistors by lithographic encoding of material thickness in chemical vapor deposition, *2D Mater.* **6**, 015017 (2018).
- [29] H. Liu, A. T. Neal, Z. Zhu, Z. Luo, X. Xu, D. Tomanek, and P. D. Ye, Phosphorene: An unexplored 2D semiconductor with a high hole mobility, *ACS Nano* **8**, 4033 (2014).
- [30] Z.-P. Ling, S. Sakar, S. Mathew, J.-T. Zhu, K. Gopinadhan, T. Venkatesan, and K.-W. Ang, Black phosphorus transistors with near band edge contact Schottky barrier, *Sci. Rep.* **5**, 18000 (2015).
- [31] L. Yu, Y.-H. Lee, X. Ling, E. J. G. Santos, Y. C. Shin, Y. Lin, M. Dubey, E. Kaxiras, J. Kong, H. Wang, and T. Palacios, Graphene/MoS₂ hybrid technology for large-scale two-dimensional electronics, *Nano Lett.* **14**, 3055 (2014).
- [32] A. Avsar, K. Marinov, G. Marin Enrique, G. Iannaccone, K. Watanabe, T. Taniguchi, G. Fiori, and A. Kis, Reconfigurable diodes based on vertical WSe₂ transistors with van der Waals bonded contacts, *Adv. Mater.* **30**, 1707200 (2018).
- [33] N. Kaushik, D. Karmakar, A. Nipane, S. Karande, and S. Lodha, Interfacial *n*-doping using an ultrathin TiO₂ layer for contact resistance reduction in MoS₂, *ACS Appl. Mat. Inter.* **8**, 256 (2016).
- [34] J. R. Chen, P. M. Odenthal, A. G. Swartz, G. C. Floyd, H. Wen, K. Y. Luo, and R. K. Kawakami, Control of Schottky barriers in single layer MoS₂ transistors with ferromagnetic contacts, *Nano Lett.* **13**, 3106 (2013).
- [35] G. Kresse and J. Furthmüller, Efficient iterative schemes for ab initio total-energy calculations using a plane-wave basis set, *Phys. Rev. B* **54**, 11169 (1996).
- [36] G. Kresse and D. Joubert, From ultrasoft pseudopotentials to the projector augmented-wave method, *Phys. Rev. B* **59**, 1758 (1999).
- [37] J. P. Perdew, K. Burke, and M. Ernzerhof, Generalized Gradient Approximation Made Simple, *Phys. Rev. Lett.* **77**, 3865 (1996).
- [38] S. Zhang, H. Y. Xiao, S. M. Peng, G. X. Yang, Z. J. Liu, X. T. Zu, S. Li, D. J. Singh, L. W. Martin, and L. Qiao, Band-Gap Reduction in (BiCrO₃)_{*m*}/(BiFeO₃)_{*n*} Superlattices: Designing Low-Band-Gap Ferroelectrics, *Phys. Rev. Appl.* **10**, 044004 (2018).
- [39] N. Wang, M. Li, H. Xiao, H. Gong, Z. Liu, X. Zu, and L. Qiao, Optimizing the thermoelectric transport properties of Bi₂O₂Se monolayer via biaxial strain, *Phys. Chem. Chem. Phys.* **21**, 15097 (2019).
- [40] J. Heyd, G. E. Scuseria, and M. Ernzerhof, Hybrid functionals based on a screened Coulomb potential, *J. Chem. Phys.* **118**, 8207 (2003).
- [41] M. Li, N. Wang, M. Jiang, H. Xiao, H. Zhang, Z. Liu, X. Zu, and L. Qiao, Improved thermoelectric performance of bilayer Bi₂O₂Se by the band convergence approach, *J. Mater. Chem. C* **7**, 11029 (2019).
- [42] L. Qiao, S. Zhang, H. Y. Xiao, D. J. Singh, K. H. L. Zhang, Z. J. Liu, X. T. Zu, and S. Li, Orbital controlled band gap engineering of tetragonal BiFeO₃ for optoelectronic applications, *J. Mater. Chem. C* **6**, 1239 (2018).
- [43] J. Klimeš, D. R. Bowler, and A. Michaelides, Van der Waals density functionals applied to solids, *Phys. Rev. B* **83**, 195131 (2011).
- [44] J. A. Wilson and A. D. Yoffe, The transition metal dichalcogenides discussion and interpretation of the observed optical, electrical and structural properties, *Adv. Phys.* **18**, 193 (1969).
- [45] A. Brown and S. Rundqvist, Refinement of the crystal structure of black phosphorus, *Acta Crystallogr.* **19**, 684 (1965).

- [46] J. Neugebauer and M. Scheffler, Adsorbate-substrate and adsorbate-adsorbate interactions of Na and K adlayers on Al(111), *Phys. Rev. B* **46**, 16067 (1992).
- [47] T. Shen, J.-C. Ren, X. Liu, S. Li, and W. Liu, Van der Waals stacking induced transition from Schottky to ohmic contacts: 2D metals on multilayer InSe, *J. Am. Chem. Soc.* **141**, 3110 (2019).
- [48] Q. Ji, C. Li, J. Wang, J. Niu, Y. Gong, Z. Zhang, Q. Fang, Y. Zhang, J. Shi, L. Liao, X. Wu, L. Gu, Z. Liu, and Y. Zhang, Metallic vanadium disulfide nanosheets as a platform material for multifunctional electrode applications, *Nano Lett.* **17**, 4908 (2017).
- [49] H. Bark, Y. Choi, J. Jung, J. H. Kim, H. Kwon, J. Lee, Z. Lee, J. H. Cho, and C. Lee, Large-area niobium disulfide thin films as transparent electrodes for devices based on two-dimensional materials, *Nanoscale* **10**, 1056 (2018).
- [50] G. Giovannetti, P. A. Khomyakov, G. Brocks, V. M. Karpan, J. van den Brink, and P. J. Kelly, Doping Graphene with Metal Contacts, *Phys. Rev. Lett.* **101**, 026803 (2008).
- [51] Y.-J. Yu, Y. Zhao, S. Ryu, L. E. Brus, K. S. Kim, and P. Kim, Tuning the graphene work function by electric field effect, *Nano Lett.* **9**, 3430 (2009).
- [52] P. N. Nirmalraj, T. Lutz, S. Kumar, G. S. Duesberg, and J. J. Boland, Nanoscale mapping of electrical resistivity and connectivity in graphene strips and networks, *Nano Lett.* **11**, 16 (2011).
- [53] Y. Liu, H. Xiao, and W. A. Goddard, Schottky-barrier-free contacts with two-dimensional semiconductors by surface-engineered MXenes, *J. Am. Chem. Soc.* **138**, 15853 (2016).
- [54] M. Naguib, O. Mashtalir, J. Carle, V. Presser, J. Lu, L. Hultman, Y. Gogotsi, and M. W. Barsoum, Two-dimensional transition metal carbides, *ACS Nano* **6**, 1322 (2012).
- [55] J. Jeon, Y. Park, S. Choi, J. Lee, S. S. Lim, B. H. Lee, Y. J. Song, J. H. Cho, Y. H. Jang, and S. Lee, Epitaxial synthesis of molybdenum carbide and formation of a Mo₂C/MoS₂ hybrid structure via chemical conversion of molybdenum disulfide, *ACS Nano* **12**, 338 (2018).
- [56] C. Xu, L. Wang, Z. Liu, L. Chen, J. Guo, N. Kang, X.-L. Ma, H.-M. Cheng, and W. Ren, Large-area high-quality 2D ultrathin Mo₂C superconducting crystals, *Nat. Mater.* **14**, 1135 (2015).
- [57] H. Xiaohui, W. Yifeng, S. Xiaodong, V. K. Arkady, S. Litao, and C. Zhongfang, 1T phase as an efficient hole injection layer to TMDs transistors: a universal approach to achieve *p*-type contacts, *2D Mater.* **5**, 031012 (2018).
- [58] Y. Liu, P. Stradins, and S.-H. Wei, Van der Waals metal-semiconductor junction: Weak Fermi level pinning enables effective tuning of Schottky barrier, *Sci. Adv.* **2**, e1600069 (2016).
- [59] C. Gong, H. Zhang, W. Wang, L. Colombo, R. M. Wallace, and K. Cho, Band alignment of two-dimensional transition metal dichalcogenides: Application in tunnel field effect transistors, *Appl. Phys. Lett.* **103**, 053513 (2013).
- [60] M. Chhowalla, H. S. Shin, G. Eda, L.-J. Li, K. P. Loh, and H. Zhang, The chemistry of two-dimensional layered transition metal dichalcogenide nanosheets, *Nat. Chem.* **5**, 263 (2013).
- [61] C. J. Carmalt, T. D. Manning, I. P. Parkin, E. S. Peters, and A. L. Hector, Formation of a new (1T) trigonal NbS₂ polytype via atmospheric pressure chemical vapour deposition, *J. Mater. Chem.* **14**, 290 (2004).
- [62] M. Farmanbar and G. Brocks, First-principles study of van der Waals interactions and lattice mismatch at MoS₂/metal interfaces, *Phys. Rev. B* **93**, 085304 (2016).
- [63] J. Kang, W. Liu, D. Sarkar, D. Jena, and K. Banerjee, Computational study of metal contacts to monolayer transition-metal dichalcogenide semiconductors, *Phys. Rev. X* **4**, 031005 (2014).
- [64] X. Zhang, Y. Pan, M. Ye, R. Quhe, Y. Wang, Y. Guo, H. Zhang, Y. Dan, Z. Song, J. Li, J. Yang, W. Guo, and J. Lu, Three-layer phosphorene-metal interfaces, *Nano Res.* **11**, 707 (2018).
- [65] P. C. Rusu, G. Giovannetti, C. Weijtens, R. Coehoorn, and G. Brocks, First-principles study of the dipole layer formation at metal-organic interfaces, *Phys. Rev. B* **81**, 125403 (2010).
- [66] P. S. Bagus, V. Staemmler, and C. Wöll, Exchangelike Effects for Closed-Shell Adsorbates: Interface Dipole and Work Function, *Phys. Rev. Lett.* **89**, 096104 (2002).
- [67] L. Li, F. Yang, G. J. Ye, Z. Zhang, Z. Zhu, W. Lou, X. Zhou, L. Li, K. Watanabe, T. Taniguchi, K. Chang, Y. Wang, X. H. Chen, and Y. Zhang, Quantum Hall effect in black phosphorus two-dimensional electron system, *Nat. Nanotechnol.* **11**, 592 (2016).